Journal of Organometallic Chemistry, 385 (1990) 131–145
Elsevier Sequoia S.A., Lausanne – Printed in The Netherlands
JOM 20586

The influence of rigid cyclic phosphine ligands in *cis*-Rh(COD)-(phosphine)$_2^+$ on inner coordination shell dynamics and catalyzed olefin hydrogenation/isomerization

R.J. Topping, L.D. Quin * and A.L. Crumbliss **

Department of Chemistry, Paul M. Gross Chemical Laboratory, Duke University, Durham, NC 27706 (U.S.A.)

(Received May 1st, 1989)

Abstract

Conformational barriers in *cis*-phosphine-rhodium(I) complexes with two pairs of isomeric ligands (Rh(COD)(L)$_2^+$, L = *anti*- or *syn*-9-phenylphosphabicyclo[4.2.1]nona-2,4,7-triene (**1** or **2**) or L = *anti*- or *syn*-9-phenylphosphatricyclo[4.2.1.0^{2,5}]nona-7-ene (**3** or **4**)) were studied by variable temperature ^{13}C, ^{31}P and ^{1}H NMR spectroscopy. Conformational barriers result from interligand steric interactions encountered during Rh–P bond rotations. These barriers are quite sensitive to individual ligand structure, with L = **1** or **3** exhibiting no conformational preference and L = **2** or **4** exhibiting a significant conformational preference within the temperature range studied. A correlation between phosphine diastereomeric *meso* form, Rh–P rotational barrier and catalytic activity/selectivity has been found. The hydrogenation and isomerization of 1-hexene homogeneously catalyzed by Rh(COD)L$_2^+$ (L = PPh$_3$, **3**, **4**) were investigated in acetone solvent in order to assess the influence of inner coordination shell steric crowding on catalytic reactivity and selectivity. The relative initial rates of catalyzed 1-hexene hydrogenation are 1/7.5/13 for L = PPh$_3$, **3**, and **4**, respectively. The rate of isomerization of 1-hexene is faster for a Rh(COD)(**3**)$_2^+$ catalyzed reaction than for a Rh(COD)(**4**)$_2^+$ catalyzed reaction. The difference in hydrogenation and isomerization rates for Rh(COD)(**3**)$_2^+$ and Rh(COD)(**4**)$_2^+$ catalyzed reactions are discussed in conjunction with the variable temperature NMR data and found to be due to the greater steric crowding imposed by **4** on the inner coordination shell of the catalyst.

---

* Current address: Department of Chemistry, University of Massachusetts at Amherst, Amherst, Massachusetts 01003 (U.S.A.)

** Address correspondence to this author.

0022-328X/90/$03.50

Introduction

Rigid cyclic phosphines capable of existing in two diastereomeric *meso* forms allow us to probe specific steric effects within the inner coordination shell of an organometallic complex. Herein we report the influence of steric effects on metal–phosphorus ligand bond rotational barriers in a series of complexes $Rh(COD)(L)_2^+$, where COD represents cycloocta-1,5-diene and L is one of two rigid asymmetric bicyclic phosphines, each of which can exist in two diastereomeric meso forms, **1**, **2** and **3**, **4**.

We have also investigated the catalytic activity of $Rh(COD)(\mathbf{3})_2^+$ and $Rh(COD)(\mathbf{4})_2^+$ with respect to 1-hexene hydrogenation/isomerization as a chemical test for the difference in inner coordination shell steric requirements for the diastereomeric ligand pair **3** and **4**. These results will allow us to correlate the steric requirements of different phosphine ligand diastereomeric *meso* forms with Rh–P bond rotation energetics and the catalytic activity/selectivity of their rhodium(I) complexes.

Use of phosphines **1**–**4** allows us to maintain the same organic moieties on the phosphorus donor atom while varying the steric bulk in the inner coordination shell of the rhodium(I). The steric bulk of these phosphines is altered by changing the position of the ligating phosphorus lone pair of electrons with respect to the C(7)–C(8) double bond. The asymmetry of the phosphine ligands is also important

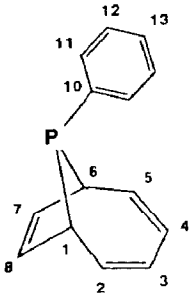

1

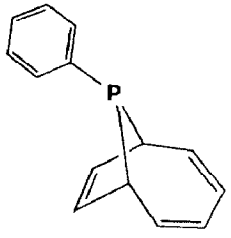

2

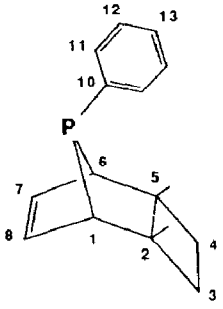

3

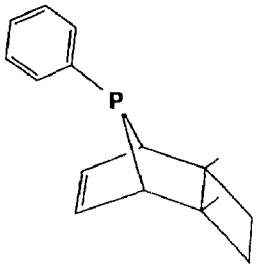

4

in that it permits detection of the rotationally related states by NMR, which is not possible by the use of $PR^1R^2R^3$ ligands which have high symmetry when $R^1 = R^2 = R^3$.

We have previously shown that variable temperature ^{31}P, ^{13}C and ^1H NMR may be applied in a readily accessible temperature range to study the energetics and conformational structure changes involved in Rh–P bond rotation [1]. In that case Rh–P bond rotation resulted from ring inversion of a cyclic Rh_2P_4 system, and the asymmetry of the $Rh(PR_3)_2$ moiety was induced by the conformation of the Rh_2P_4 ring system. In this report, temperature dependent ^1H, ^{13}C and ^{31}P NMR data are used to establish the dynamic nature of the Rh–P bond rotations in $Rh(COD)(L)_2^+$, where L = **1**–**4**.

Rhodium complexes with phosphine ligands have long been studied for their activity as homogeneous catalysts [2]. These rhodium-phosphine complexes have shown considerable activity towards catalyzing olefin hydrogenation and isomerization reactions. The activity/selectivity of these catalysts may often be controlled by the choice of phosphine ligands bound to the metal. To our knowledge, the specific influence of rigid cyclic phosphines locked in *syn* or *anti* configurations such as described here has not been investigated with respect to rhodium complex catalytic activity and selectivity.

The gross mechanistic features of the hydrogenation of 1-hexene, homogeneously catalyzed by $Rh(COD)(L)_2^+$ complexes (L = phosphine), have been investigated by Schrock et al. [3], and later by Collman et al. [4] and Anton and Crabtree [5]. Schrock et al. [3] found that olefin hydrogenation and isomerization rates increased with increasing phosphine ligand basicity in the order $PPh_3 < PPh_2Me < PPhMe_2 < PMe_3$. However, within this series of phosphines the ligand steric bulk decreases as the basicity increases. Steric interactions within the inner coordination shell are known to influence the stability of the Rh^I–olefin bond [6] and the distribution of olefin isomerization products [7,8,9]. Thus it may be expected that in the hydrogenation/isomerization catalytic cycle the stability of the reactive olefin complex, as well as the intermediate alkyl complex, will be influenced by the steric requirements of the ancillary phosphine ligands.

Experimental

Materials

Dichloromethane was freshly distilled from P_2O_5 prior to use. $RhCl_3 \cdot 6H_2O$ was purchased from Strem Chemicals and used without further purification. All other chemicals were purchased from Aldrich Chemical Company and were purified by standard procedures when necessary. Acetone was freshly distilled in a N_2 atmosphere from 4A molecular sieves prior to each catalytic run. 1-Hexene was distilled from CaH_2 prior to use.

$[Rh(COD)(PPh_3)_2]BF_4$ [6] was prepared according to literature methods; m.p. 195 °C (dec.) (Lit. [10] m.p. 192–194 °C). *syn* and *anti*-9-Phenyl-9-phosphabicyclo-[4.2.1]nona-2,4,7-triene (**1** and **2**) were prepared and purified as described in the literature [11]. Their rhodium complexes were prepared by adding a stoichiometric amount of **1** or **2** by syringe to $[Rh(COD)_2]BF_4$ [12] in CH_2Cl_2 in a N_2 atmosphere, followed by the slow addition of diethyl ether to precipitate orange air-stable

crystals of $[Rh(COD)(\mathbf{1})_2]BF_4$ (60% yield; m.p. 170 °C (dec.)) or $[Rh(COD)(\mathbf{2})_2]BF_4$ (76% yield; m.p. 165 °C (dec.)).

anti-9-Phenyl-9-phosphatricyclo[4.2.1.0^{2,5}]nona-7-ene (3). *anti*-9-Phenyl-9-phosphatricyclo[4.2.1.0^{2,5}]nona-3,7-diene-9-oxide (**5**) was prepared by the method of Turnblom and Katz [13] by UV photolysis of *syn*-9-phenyl-9-phosphabicyclo[4.2.1]-nona-2,4,7-triene-9-oxide. Acetic acid (0.40 ml, 7.0 mmol) was added to a suspension of **5** (0.50 g, 2.2 mmol) and finely powdered dipotassium azodicarboxylate [14] (0.47 g, 2.4 mmol) in 50 ml of dry CH_2Cl_2. The suspension was stirred in a N_2 atmosphere at 20 °C for three days. The resulting white precipitate (potassium acetate) was removed by filtration. The solution was concentrated under reduced pressure whereupon a white solid (product) was isolated. Recrystallization from benzene gave 0.39 g (77% yield) of *anti*-9-phenyl-9-phosphatricyclo[4.2.1.0^{2,5}]nona-7-ene-9-oxide (**6**), m.p. 183–184 °C. ^{31}P NMR ($CDCl_3$): $\delta + 93.1$; ^{13}C NMR ($CDCl_3$) (J in Hz): δ 22.4 (d, J(PC) 9.3, C(3,4)), 34.0 (d, J(PC) 28.6, C(2,5)), 43.2 (d, J(PC) 65.4, C(1,6)), 128.6 (d, J(PC) 10.4, C(12)), 129.0 (d, J(PC) 9.9 C(11)), 131.3 (d, J(PC) 2.2, C(13)), 131.7 (d, J(PC) 3.8, C(7,8)), 132.5 (d, J(PC) 74.1, C(10)); ^1H NMR ($CDCl_3$, 300 MHz, J in Hz) $\delta + 7.5$–7.8 (m, aryl), 6.92 (dt, ^3J(PH) 10.9, ^3J(HH) = ^4J(HH) = 3.5, H(7,8)), 3.38 (m, H(1,6)), 2.71 (m, H(2,5)), 1.97 (m, *exo*-H(3,4)), 1.44 (m, *endo*-H(3,4)). Anal. Found: C, 73.18; H, 6.55; P, 13.73. $C_{14}H_{15}OP$ calcd.: C, 73.03; H, 6.57; P, 13.45%. The oxide **6** (0.290 g, 1.26 mmol) was reduced by a procedure similar to that reported previously [15,16] to give 0.24 g (89%) of a white oily solid, **3**. Pyridine was present during the reduction to prevent inversion at phosphorus, which was confirmed by the large upfield ^{31}P chemical shift of **3** relative to the *syn* isomer **4** [16]. The product showed no impurities by ^{13}C or ^{31}P NMR spectroscopy, and was used without further purification. ^{31}P NMR ($CDCl_3$): $\delta + 56.6$; ^{13}C NMR ($CDCl_3$) (J in Hz): δ 19.7 (s, C(3,4)), 39.2 (d, J(PC) 2.2, C(2,5)), 46.0 (d, J(PC) 11.5, C(1,6)), 126.5 (s, C(13)), 128.1 (d, J(PC) 8.3, C(12)), 128.4 (d, J(PC) 22.0, C(11)), 133.9 (d, J(PC) 20.9, C(7,8)), 141.7 (d, J(PC) 38.4, C(10)). Elemental analysis was obtained from the rhodium complex derivative prepared from $[Rh(COD)_2]BF_4$ [12] as described above. $[Rh(COD)(\mathbf{3})_2]BF_4$; 88% yield of yellow crystals, m.p. 180 °C (dec.); Anal. Found: C, 59.28; H, 5.83; P, 8.60. $C_{36}H_{42}BF_4P_2Rh$ calcd.: C, 59.53; H, 5.83; P, 8.53%.

syn-9-Phenyl-9-phosphatricyclo[4.2.1.0^{2,5}]nona-7-ene (4). *syn*-9-Phenyl-9-phosphatricyclo[4.2.1.0^{2,5}]nona-3,7-diene oxide (**7**) was prepared by isomerization of *anti*-9-phenyl-9-phosphatricyclo[4.2.1.0^{2,5}]nona-3,7-diene oxide (**5**) as described previously [17]. *syn*-9-Phenyl-9-phosphatricyclo[4.2.1.0^{2,5}]nona-7-ene oxide (**8**) was prepared by the dipotassium azodicarboxylate reduction of **7** (as described above for **5**) in 87% yield; m.p. 113–115 °C. ^{31}P NMR ($CDCl_3$): $\delta + 86.6$; ^{13}C NMR ($CDCl_3$) (J in Hz): δ 20.2 (d, J(PC) 9.4 , C(3,4)), 35.73 (d, J(PC) 18.1, C(2,5)), 43.6 (d, J(PC) 63.7, C(1,6)), 126.9 (d, J(PC) 11.0, C(12), 128.1 (d, J(PC) 83.5, C(10)), 130.0 (d, J(PC) 2.7, C(13)), 130.1 (d, J(PC) 11.0, C(7,8)), 132.0 (d, J(PC) 7.7, C(11)); ^1H NMR ($CDCl_3$, 300 MHz) (J in Hz): δ 7.24–7.40, 7.54–7.64 (m, aryl), 6.33 (dt, ^3J(PH) 11.8, ^3J(HH) = ^4J(HH) = 4.5, H(7,8)), 3.38 (m, H(2,5), 3.19 (m, H(1,6)), 2.08 (m, *exo*-H(3,4)), 1.32 (m, *endo*-H(3,4)). Anal. Found: C, 72.80; H, 6.66; P, 13.46. $C_{14}H_{15}OP$ calcd.: C, 73.03; H, 6.57; P, 13.45%. The oxide **8** (0.427 g, 1.86 mmol) was reduced by a procedure similar to that reported previously [15,16] to give 0.37 g (94%) of a white oily solid **4**. Pyridine was present during the reduction to prevent inversion at phosphorus, which was confirmed by the large downfield ^{31}P chemical

shift of **4** relative to the *anti* isomer **3** [16]. The product showed no impurities by ^{13}C or ^{31}P NMR spectroscopy, and was used without further purification. ^{31}P NMR ($CDCl_3$) δ +129.7; ^{13}C NMR ($CDCl_3$) (J in Hz): δ 22.3 (d, J(PC) 12.1, C(3,4)), 38.0 (d, J(PC) 38.3, C(2,5)), 48.4 (d, J(PC) 9.9, C(1,6)), 127.2 (s, C(13)), 127.6 (d, J(PC) 4.4, C(12)), 131.9 (d, J(PC) 13.2, C(11)), 133.5 (d, J(PC) 5.5, C(7,8)), 138.5 (d, J(PC) 28.7, C(10)). Elemental analysis was obtained from the rhodium complex derivative prepared from $[Rh(COD)_2]BF_4$ [12] as described above. $[Rh(COD)(\mathbf{4})_2]BF_4$: 65% yield of brown crystals, m.p. 160 °C (dec.); Anal. Found: C, 59.05; H, 4.96; B, 1.47; F, 10.69; P, 8.05; Rh, 14.09. $C_{36}H_{42}BF_4P_2Rh$ calcd.: C, 59.53; H, 5.83; B, 1.49; F, 10.46; P, 8.53; Rh, 14.17%.

Methods

Proton and carbon NMR spectra were recorded using a Varian XL-300 spectrometer operating at 299.94 and 75.43 MHz, respectively. Phosphorus NMR spectra were recorded using a JEOL FX-90Q spectrometer operating at 36.20 MHz. Internal deuterium lock was used for all NMR spectral acquisitions. Proton or carbon resonances were referenced as positive chemical shifts if downfield from tetramethylsilane. Phosphorus resonances were referenced as positive chemical shifts if downfield from external 85% aqueous H_3PO_4. Broad band proton decoupling was employed for all carbon and phosphorus spectra. Elemental analyses were performed by MHW Laboratories, Phoenix, AZ, or Galbraith Laboratories, Knoxville, TN.

Activation parameters were calculated by the method of Shanan–Atidi and Bar–Eli [18]. Standard deviations were calculated based on the estimated experimental error in measurement of T_c and $\Delta\nu$.

Catalytic hydrogenation reactions were carried out at a constant H_2 pressure (1 atm) in a 100 ml fluted reaction flask attached to a 100 ml pressure-equalizing gas buret. The reaction flask was charged with solid catalyst (1.2×10^{-5} mol $[Rh(COD)(\mathbf{3})_2]BF_4$ or $[Rh(COD)(\mathbf{4})_2]BF_4$; 2.4×10^{-5} mol $[Rh(COD)(PPh_3)_2]BF_4$) and the side arm charged with 20 ml of dry acetone and 2.0 ml of freshly distilled 1-hexene. The contents of the side arm flask were deoxygenated by several freeze-thaw cycles. H_2 was introduced to the flask and buret at a slight positive pressure (2 torr), and the side arm flask was rotated to introduce solvent and substrate into the reaction flask. The solution was magnetically stirred while thermostated at 25 °C. Reactant/product composition during the course of the reaction was determined by periodically removing aliquots from the reaction mixture by syringe through a septum-fitted stopcock opening in the reaction flask. Aliquots were flash evaporated under reduced pressure with the volatiles (solvent, substrate and products) trapped at liquid N_2 temperature. This volatile fraction was quantitatively analyzed by its ^1H NMR (Varian XL-300) spectrum to determine relative amounts of 1-hexene, isomeric internal olefin, and n-hexane. The ^1H NMR resonances for 1-hexene were distinguished from the envelope of resonances for the isomeric olefins and allowed determination of their relative amounts. The relative amount of hexane was determined by integration of the combined, terminal methyl resonance and subtraction of the contribution by the olefin fractions. No acetone hydrogenation product (2-propanol) was detected at anytime during these experiments.

Results

Table 1 summarizes ^{31}P chemical shift data for the phosphines **1–4** and their rhodium(I) complexes, Rh(COD)(phosphine)$_2^+$. The determination of phosphorus configuration by ^{31}P NMR is well documented [16]. The free ligand diastereomers show significant differences in their ^{31}P chemical shifts. The *anti* isomers (**1** and **3**) exhibit a ^{31}P chemical shift which is upfield relative to the chemical shift for the corresponding *syn* isomers (**2** and **4**). In all cases coordination to rhodium(I) results in a downfield shift of the ^{31}P resonance. The relative difference in chemical shift between *anti* and *syn* diastereomers is maintained upon coordination. In all of the complexes studied there is no evidence for non-coordinated phosphine in solution.

The dynamic properties of Rh(COD)(L)$_2^+$ in solution can be inferred from their temperature dependent NMR spectra. Rh(COD)(L)$_2^+$ (L = **1**, **2** or **3**) exhibit a sharp temperature-independent ^{31}P doublet resonance over the temperature range from −50 to +25 °C. Rh(COD)(**4**)$_2^+$, however, exhibits a temperature dependent ^{31}P spectrum as shown in Fig. 1. Variable temperature ^{31}P NMR spectra obtained over the range from −50 to +64 °C provide a coalescence temperature (T_c +10 °C) and a signal separation at the limit of no exchange (−50 °C) of 110 Hz for the two doublets. A distribution ratio of 3 to 1 (also established by ^1H NMR; see below) for the two species (X and Y, respectively) allows the calculation of the free energies of activation [18] for the interconversions of these species as $\Delta G^{\ddagger}_{283}$ (X → Y) = 14.1 ± 0.5 kcal/mol and $\Delta G^{\ddagger}_{283}$ (Y → X) = 13.5 ± 0.5 kcal/mol.

Rh(COD)(**4**)$_2^+$ also exhibits a temperature dependent ^1H NMR spectrum, as shown in Fig. 2. A 3 to 1 distribution ratio for species X and Y may be established from sets of phosphine ligand olefinic resonances at −30 °C. Each set of resonances consists of two peaks of equal intensity. The resonances for the minor species (Y) are at δ 6.25 and 6.50 ppm, while the resonances of the major species (X) are at δ 6.10 and 6.60 ppm. Spectra obtained at higher temperatures exhibit line broadening and coalescence of both sets of resonances. The ^{13}C NMR spectrum for Rh(COD)(**4**)$_2^+$ was too complicated for assignment when measured at −40 or +30 °C.

Rh(COD)(**1**)$_2^+$ and Rh(COD)(**3**)$_2^+$ exhibit temperature independent ^{13}C NMR spectra with typical phosphorus-coupled AA'X resonances (A = ^{31}P; X = ^{13}C) as shown in Table 2. However, Rh(COD)(**2**)$_2^+$ exhibits a temperature dependent ^{13}C NMR spectrum for resonances of the COD olefinic and methylene carbons, the

Table 1

^{31}P NMR chemical shifts for phosphines and their rhodium complexes [Rh(COD)(phosphine)$_2$]BF$_4$

Phosphine	δ(^{31}P)	
	Free	Complex (^1J(Rh–P))
1	−78.0 [a]	−15.9(147) [c]
2	−13.5 [b]	+13.6(151) [c]
3	+56.6 [a]	+95.1(147) [c]
4	+129.7 [a]	+143.6(137) [d]
		144.1(137) [e], 141.1(137) [e]

[a] 25 °C, $CDCl_3$. [b] 25 °C, C_6D_6. [c] 25 °C, CD_2Cl_2. [d] 64 °C, CD_2Cl_2. [e] −50 °C, CD_2Cl_2.

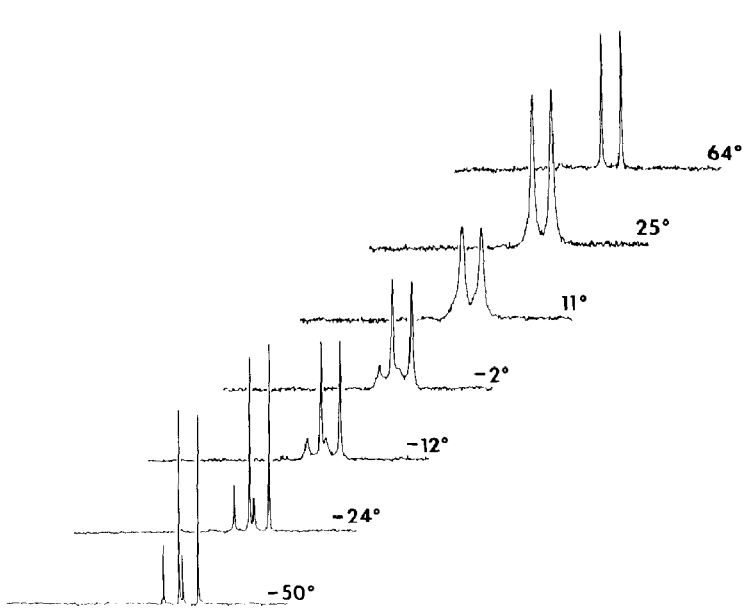

Fig. 1. Variable temperature ^{31}P NMR spectra of Rh(COD)(**4**)$_2^+$ in CD_2Cl_2 at 36.20 MHz.

bridgehead sp^3 carbons C(1,6), and the olefinic carbons C(7,8) and C(3,4). In each case, the temperature dependence involves a pair of resonances at low temperature which coalesce and sharpen at higher temperature. These spectra are presented in Fig. 3. All other resonances appear as resolved AA'X triplet resonances at all temperatures examined. ^{13}C peak assignments are listed in Table 2 and are compared with the coordinated phosphine diastereomer complex Rh(COD)(**1**)$_2^+$. Also included in footnotes to Table 2 are coalescence temperatures for each of the temperature-dependent resonances, the peak separations at slow exchange ($\Delta\nu$) and the $\Delta G^{\ddagger}$ values calculated at each coalescence temperature for Rh(COD)(**2**)$_2^+$. A plot of $\Delta G^{\ddagger}$ versus T yields $\Delta H^{\ddagger} = 9.0\ (\pm 2)$ kcal/mol and $\Delta S^{\ddagger} = -12\ (\pm 10)$ eu.

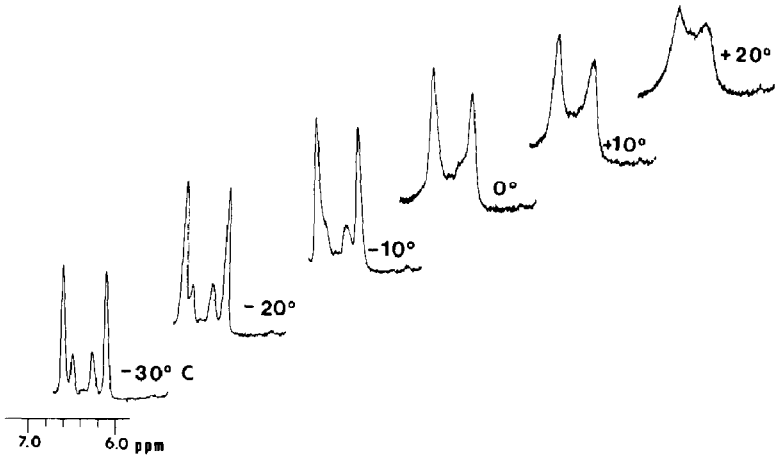

Fig. 2. Variable temperature ^1H NMR spectra of the phosphine ligand olefinic protons of Rh(COD)(**4**)$_2^+$ in CD_2Cl_2 at 299.94 MHz.

Table 2

^{13}C NMR data for rhodium complexes $Rh(COD)(L)_2^+$ [a]

C-atom [c]	$\delta(^{13}C)$ ($\lvert {}^nJ(PC) + {}^{n+2}J(P'C) \rvert$) [b]				
	L = **1**	L = **2** [d]	L = **2** [e]	L = **3**	L = PPh_3
1,6	39.9(10.5)	47.0/41.1 [a](0)	44.0(0)	45.5(27.4)	–
2,5	132.0(5.0)	133.3(0)	133.7(17)	33.7(8.2)	–
3,4	128.2(0)	126.9/126.0 [f](0)	127.0(0)	20.5(5.0)	–
7,8	122.4(5.5)	121.3/120.2 [f](0)	121.3(0)	133.5(13.2)	–
ipso	[f]	[f]	[f]	133.9(10.0) [g]	130.1(44.0)
ortho	132.9(30)	130.9(0)	131.3(0)	129.9(9.8)	134.0(11.0)
meta	128.9(4.0)	129.0(0)	129.3(20)	129.5(7.8)	128.6(9.9)
para	131.0	130.9	131.2	130.7	130.9
COD olefinic	97(m)	99.0/92.0 [k]	96	97.3(m)	99.2(m)
COD methylene	31.7	31.7/29.8 [l]	31	30.9	30.5

[a] Obtained in CD_2Cl_2 at 25 °C unless otherwise noted. Recorded with a Varian XL-300 spectrometer operating at 75.43 MHz. [b] Coupling assigned for AA'X triplet pattern. [c] See text for structure and numbering scheme. [d] $T = -40$ °C. [e] T +30 °C. [f] Not observed. [g] Doublet of triplets, ^2J(Rh–C) 2 Hz, recorded using a JEOL-FX90Q spectrometer operating at 36.20 MHz. [h] T_c 293(±3) K; $\Delta\nu$ 463 Hz; $\Delta G^{\ddagger}$ 13.10 (±0.14) kcal/mol. [i] T_c 263(±2) K; $\Delta\nu$ 81 Hz; $\Delta G^{\ddagger}$ 12.62 (±0.05) kcal/mol. [j] T_c 271(±2) K; $\Delta\nu$ 96 Hz; $\Delta G^{\ddagger}$ 12.92 (±0.10) kcal/mol. [k] T_c 293(±3) K; $\Delta\nu$ 517 Hz; $\Delta G^{\ddagger}$ 13.04 (±0.14) kcal/mol. [l] T_c 275(±2) K; $\Delta\nu$ 128 Hz; $\Delta G^{\ddagger}$ 12.96 (±0.11) kcal/mol.

The low temperature ^1H NMR spectrum of $Rh(COD)(\mathbf{2})_2^+$ shows coalescence upon warming, but assignments are complicated by P–H and H–H couplings, likely resulting in resonances with non-first order couplings.

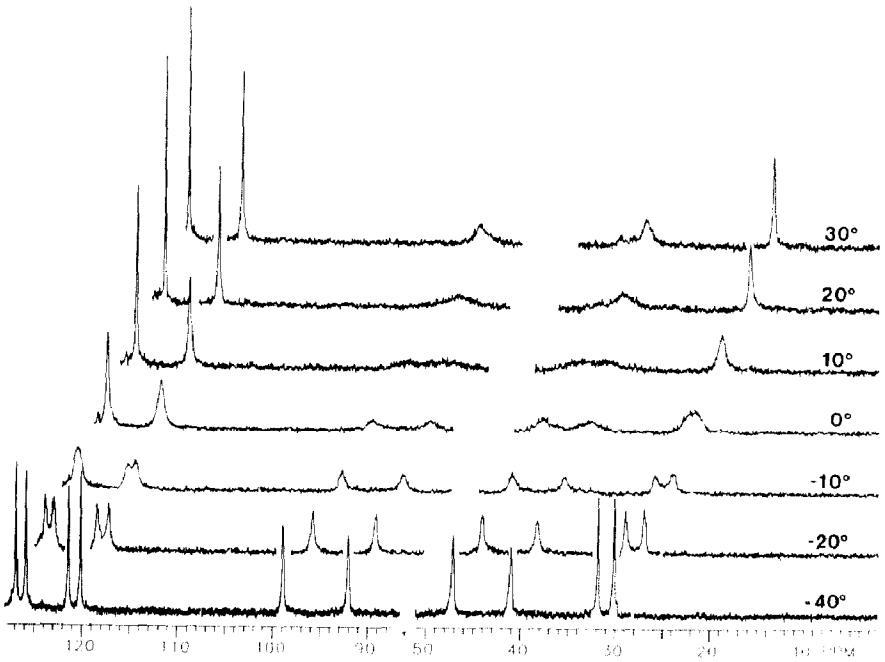

Fig. 3. Variable temperature ^{13}C NMR spectra of $Rh(COD)(\mathbf{2})_2^+$ in $CDCl_3$ at 75.43 MHz.

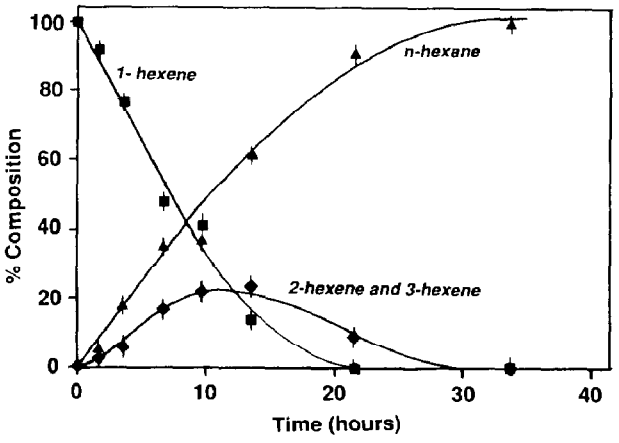

Fig. 4. Plot of percent composition of n-hexane and hexene isomers from the hydrogenation/isomerization of 1-hexene catalyzed by $Rh(COD)(PPh_3)_2^+$ in acetone vs. time. Conditions: $[Rh(COD)(PPh_3)_2]BF_4$ 1.1×10^{-3} *M*; $[1\text{-}C_6H_{12}]$ 7.27×10^{-1} *M*; $P(H_2)$ 1 atm; *T* 25 °C.

$Rh(COD)(\mathbf{3})_2^+$ and $Rh(COD)(\mathbf{4})_2^+$ were used as catalysts for the hydrogenation of 1-hexene in acetone at 25 °C. Data were also obtained using $Rh(COD)(PPh_3)_2^+$ as a catalyst for the purpose of making a direct comparison with the literature [2,3]. The disappearance of 1-hexene and the appearance of n-hexane, 2-hexene and 3-hexene were monitored as a function of time for each catalyst. Representative plots of these data are given in Figs. 4–6 at conditions where the initial 1-hexene/catalyst ratio was 10^3, *T* 25 °C and $P(H_2)$ 1 atm. Table 3 lists the initial second order rate constants and relative reactivities for hexane produced for each catalyst.

The reaction mixtures remained homogeneous throughout the course of the reaction. The color of the reaction solutions faded considerably, consistent with the formation of $RhH_2(L)_2(S)_x^+$ (S = solvent), similar to that observed by others in methanol [19] and acetone [3]. Presumably, in the initial induction phase of the

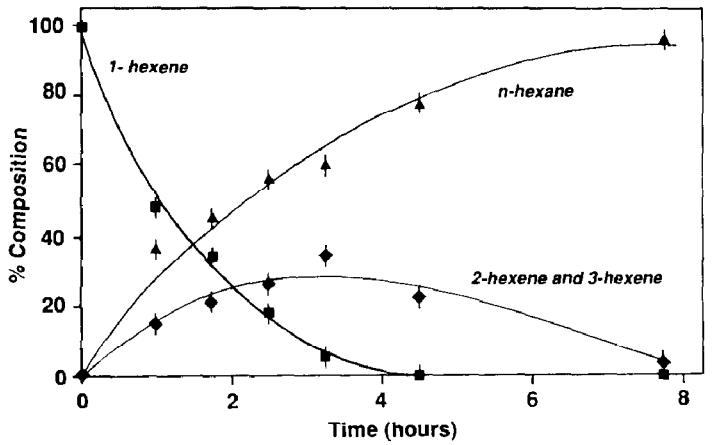

Fig. 5. Plot of percent composition of n-hexane and hexene isomers from the hydrogenation/isomerization of 1-hexene catalyzed by $Rh(COD)(\mathbf{4})_2^+$ in acetone vs. time. Conditions: $[Rh(COD)(\mathbf{4})_2]BF_4$ 5.46×10^{-4} *M*; $[1\text{-}C_6H_{12}]$ 7.27×10^{-1} *M*; $P(H_2)$ 1 atm; *T* 25 °C.

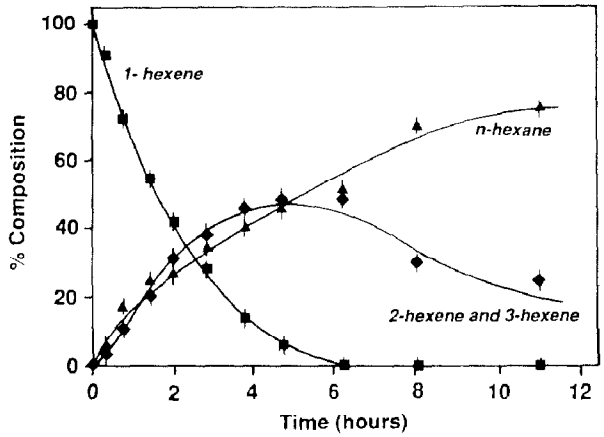

Fig. 6. Plot of percent composition of n-hexane and hexene isomers from the hydrogenation/isomerization of 1-hexene catalyzed by $Rh(COD)(\mathbf{3})_2^+$ in acetone vs. time. Conditions: $[Rh(COD)(\mathbf{3})_2]BF_4$ 5.46×10^{-4} *M*; $[1\text{-}C_6H_{12}]$ 7.27×10^{-1} *M*; $P(H_2)$ 1 atm; *T* 25 °C.

reaction, the COD ligand is hydrogenated, producing the catalytically active $RhH_2(L)_2(S)_x^+$ [19].

In comparing catalysis by $RhH_2(\mathbf{4})_2S_x^+$ and $RhH_2(PPh_3)_2S_x^+$, it can be seen that the rates of hydrogenation and isomerization are much faster in the former case (see Figs. 4 and 5). Also, in both cases the initial rate of formation of n-hexane is approximately twice as fast as the initial rate of formation of the combined internal isomeric hexenes. The maximum percent composition of these isomeric hexenes is 25% for $RhH_2(PPh_3)_2S_x^+$ and 35% for $RhH_2(\mathbf{4})_2S_x^+$.

The rates of disappearance of 1-hexene catalyzed by $RhH_2(\mathbf{3})_2S_x^+$ and $RhH_2(\mathbf{4})_2S_x^+$ systems are similar (Figs. 5 and 6). However, the initial distribution of products for the two catalysts is different. $RhH_2(\mathbf{4})_2S_x^+$ catalyzes the formation of n-hexane at a faster rate (Table 3), while $RhH_2(\mathbf{3})_2S_x^+$ catalyzes the formation of the combined internal hexene isomers at a faster rate (Figs. 5 and 6). In fact, for the $RhH_2(\mathbf{3})_2S_x^+$ catalyst the initial rates of formation of n-hexane and of the combined internal isomers are approximately equal. The maximum percent composition of combined internal hexene isomers is 50% and the rate of disappearance of this fraction is much slower than the rate of disappearance of 1-hexene at comparable substrate concentrations. After 11 hours, only 75% of all species had been converted to n-hexane in the $RhH_2(\mathbf{3})_2S_x^+$ catalyzed reaction (Fig. 6).

Table 3

Relative reactivities of catalytic precursors for hexane production in acetone

Precursor	10^2 k/M^{-1} s^{-1} [a]	*R* [b]
$[Rh(COD)(PPh_3)_2]BF_4$	1.3	1
$[Rh(COD)(\mathbf{3})_2]BF_4$	9.8	7.5
$[Rh(COD)(\mathbf{4})_2]BF_4$	17	13

[a] Second order rate constant for hexane formation from 1-hexene obtained from initial rates when $P(H_2)$ 1 atm and *T* 25 °C; estimated error ±10%. [b] Relative reactivities based on second order rate constants from column 2.

Discussion

The assessment of ligand size and shape necessary to influence the mobility about the ligand donor atom–metal bond is made possible by the use of rigid cyclic phosphines which incorporate asymmetry about the Rh–P bond axis. This asymmetry allows detection of the rotationally related states by variable temperature NMR.

The *cis*-Rh(COD)$(L)_2^+$ coordination structure is maintained in solution for all of the complexes reported here. This is evidenced by the magnitude of ^1J(RhP) and the absence of non-coordinated ligand resonances of any kind in the NMR spectra of the complexes at any temperature studied. The AA′X patterns (A = ^{31}P, X = ^{13}C) in the ^{13}C NMR spectra of these species are consistent with this structural assignment. This precludes processes involving ligand exchange or Rh coordination geometry modifications as the source of the observed solution dynamics. Thus the solution dynamic processes are interpreted as arising from Rh–P bond rotation.

At 20 °C, the ^{13}C NMR spectrum of Rh(COD)$(PPh_3)_2^+$ consists of sharp, resolved resonances (Table 2). The triplet pattern for each carbon site of the phenyl rings is assigned as an AA′X pattern. The resolved multiplet for the olefinic COD carbons most likely results from coupling to ^{103}Rh and the two chemically equivalent ^{31}P nuclei. Thus the molecule has essentially C_{2v} symmetry on the NMR time scale at 20 °C. These observations indicate chemical equivalence of all phenyl substituents as well as COD olefinic carbons and thus a rapid rate of ligand site "exchange" due to low barriers to Rh–P bond rotation. Similar line shapes are observed in the ^{13}C NMR spectra of Rh(COD)(**1**)$_2^+$ and Rh(COD)(**3**)$_2^+$ (Table 2). However, the ^{13}C NMR spectrum of Rh(COD)(**2**)$_2^+$ (Table 2, Fig. 3) consists mostly of broad, featureless resonances at 20 °C, while the ^{13}C NMR spectrum of Rh(COD)(**4**)$_2^+$ is considerably more complex and also featureless.

The temperature independence of the ^{31}P, ^{13}C and ^{1}H NMR spectra of Rh(COD)(**1**)$_2^+$ and Rh(COD)(**3**)$_2^+$ are due to low activation barriers to Rh–P bond rotation processes over the temperature range studied. For Rh(COD)(**2**)$_2^+$ and Rh(COD)(**4**)$_2^+$, however, the rates of conformational exchange are slow enough to allow the dynamic processes to be observed by NMR and to allow calculation of the $\Delta G^{\ddagger}$ values for these processes. The resolved equal intensity resonances in the ^{13}C NMR spectrum of Rh(COD)(**2**)$_2^+$ (Fig. 3) and the ^{1}H NMR spectrum of Rh(COD)(**4**)$_2^+$ (Fig. 2) indicate that $\Delta G° = 0$ for the species involved in the exchange process of each complex. For Rh(COD)(**4**)$_2^+$, however, the observation of two doublets of unequal intensity in the ^{31}P NMR spectrum (Fig. 1) and two sets of resonances of unequal intensity in the ^{1}H NMR spectrum (Fig. 2) indicates that an additional equilibrium, for which $\Delta G° \neq 0$, is also observed.

For those solution dynamic processes ($\Delta G° = 0$) involving Rh(COD)(**2**)$_2^+$ in which the ^{31}P NMR spectra are temperature independent, the phosphorus nuclei in the observed exchanging conformers retain an equivalent chemical environment. Thus the exchanging conformers must be related by C_2 symmetry which bisects the P–Rh–P moiety. However, the temperature dependence of the ^{13}C and ^{1}H NMR spectra of Rh(COD)(**2**)$_2^+$ suggest that the C_2 symmetry element does not bisect the C(1)–P–C(6) moiety. The direct I $\rightleftharpoons$ I′ conformational exchange illustrated in Scheme 1 represents such a process. For Rh(COD)(**2**)$_2^+$, the forms II and II′ may represent highly energetic transition states for the I $\rightleftharpoons$ I′ interconversion.

The temperature dependence of the ^{31}P NMR spectrum and the additional

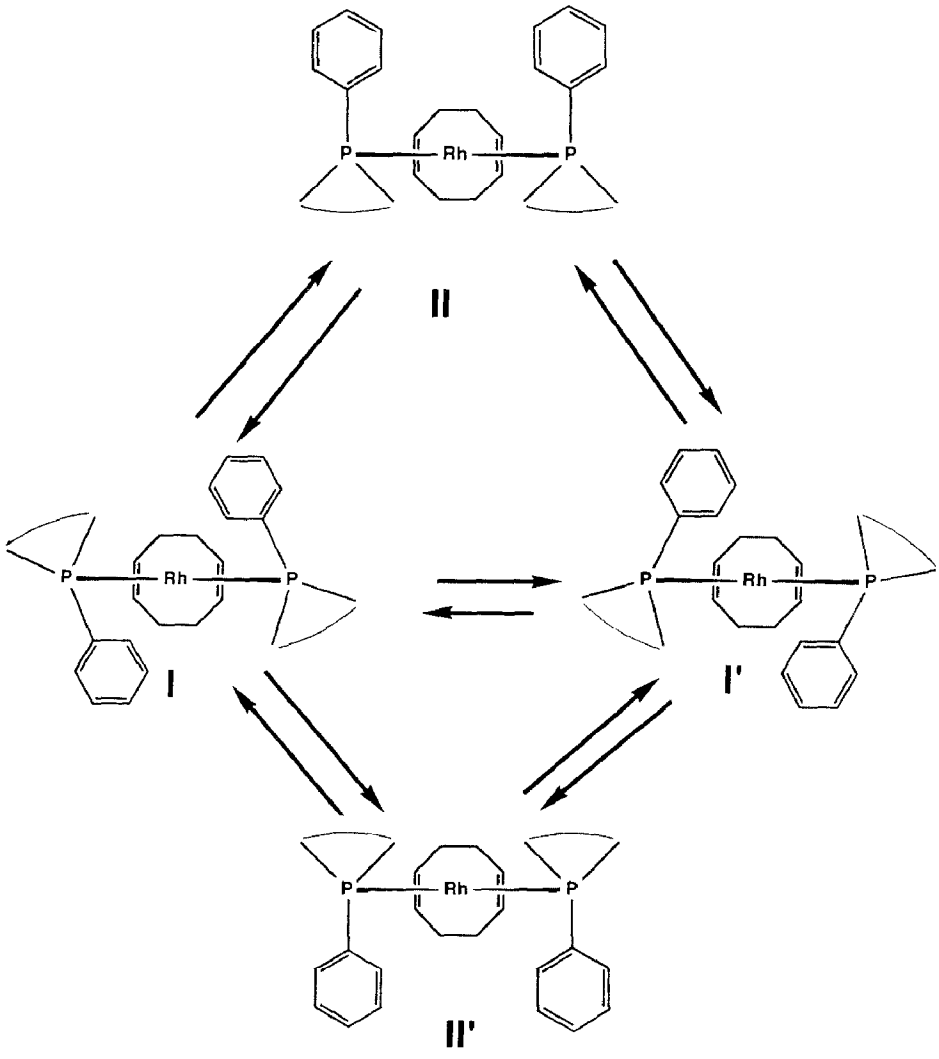

Scheme 1

complexity of the ^{1}H NMR spectrum of Rh(COD)(**4**)$_2^+$ indicate that an additional process occurs in which ΔG° for the exchanging conformers is non-zero. Observable conformational exchange between metal complex conformers I and II or I′ and II′ as shown in Scheme 1 is consistent with these observations. Relative stabilities of the two conformers I and I′, as well as the two conformers II and II′, should be identical and hence $\Delta G^\circ = 0$ for the processes I $\rightleftharpoons$ I′ and II $\rightleftharpoons$ II′. However, for steric reasons the II and II′ conformers are likely to be less stable than the I and I′ conformers and hence $\Delta G^\circ \neq 0$ for the I $\rightleftharpoons$ II and I′ $\rightleftharpoons$ II′ exchanges. That is, for the Rh(COD)(**4**)$_2^+$ complex, the forms II and II′ now represent energetically stable intermediates in the conversion I $\rightleftharpoons$ I′. Each of the two pairs (I, I′ or II, II′) of conformers for which $\Delta G^\circ = 0$ gives rise to a separate doublet in the low temperature ^{31}P NMR spectrum. The conformers I and I′ are assigned as the major species, exhibiting $\delta(^{31}P)$ 141.1 ppm, and II and II′ the minor species at $\delta(^{31}P)$ 144.1.

The restriction of the Rh–P bond rotations of $Rh(COD)(\mathbf{2})_2^+$ and $Rh(COD)(\mathbf{4})_2^+$ relative to complexes of their diastereomeric phosphines, $Rh(COD)(\mathbf{1})_2^+$ and $Rh(COD)(\mathbf{3})_2^+$ respectively, results from the differences in interligand interactions encountered during rotation. In $Rh(COD)(\mathbf{2})_2^+$, the axis of Rh–P rotation is oriented (due to the stereochemistry at P) such that the four-carbon diene moieties of the ligands must encounter either each other or the phenyl ring of the other ligand during one complete Rh–P rotation. The interligand interactions encountered in $Rh(COD)(\mathbf{1})_2^+$ involve the smaller C(7)–C(8) olefin moiety. The relatively weaker interligand interactions and structural deformations permit facile Rh–P rotation in $Rh(COD)(\mathbf{1})_2^+$; therefore, the small $\Delta G^{\ddagger}$ values do not permit different conformer detection by NMR in the temperature range studied. Similarly, interligand interactions of the cyclobutane moieties in $Rh(COD)(\mathbf{4})_2^+$ provide a significant energy barrier to Rh–P rotation relative to the interligand interactions of the C(7)–C(8) moieties in $Rh(COD)(\mathbf{3})_2^+$.

The difference in conformational dynamics between $Rh(COD)(\mathbf{2})_2^+$ and $Rh(COD)(\mathbf{4})_2^+$ may be best explained by the difference in ligand width, defined here as the intraligand C(2)–C(5) interatomic distance. In $Rh(COD)(\mathbf{4})_2^+$ the ligands **4** are sufficiently narrow to allow an energetically favorable parallel orientation (conformers II and II′ in Scheme 1). The analogous conformation in $Rh(COD)(\mathbf{2})_2^+$ experiences more conflicting intraligand (C(2,5)–C′(2,5)) interactions, due to the greater width of **2**, making such a conformation highly energetic. In the case of $Rh(COD)(\mathbf{2})_2^+$ the structures II and II′ in Scheme 1 represent probable transition states rather than intermediates as seen in $Rh(COD)(\mathbf{4})_2^+$ for the $I \rightleftharpoons I'$ conformational exchange process.

The contrast between the temperature independent NMR spectra observed for $Rh(COD)(\mathbf{3})_2^+$ and the temperature dependent NMR spectra observed for $Rh(COD)(\mathbf{4})_2^+$ has been interpreted in terms of the different steric bulk brought into the inner coordination shell by the two stereoisomeric ligands **3** and **4**. The results of the hydrogenation and isomerization of 1-hexene catalyzed by $Rh(COD)(\mathbf{3})_2^+$ and $Rh(COD)(\mathbf{4})_2^+$ were found to be consistent with the dynamic NMR studies and serve as a catalytic activity/selectivity probe to evaluate the influence of ligand steric bulk on reactions occurring within the inner coordination shell of an organometallic complex.

The consumption of 1-hexene in the $Rh(COD)(L)_2^+$ catalyzed reactions results from both a hydrogenation to n-hexane and isomerization to internal isomers (mostly 2-hexene). The $L = PPh_3$ complex was investigated to serve as a comparison with data available in the literature. The general features of the plots of percent composition for the catalyst systems comprised of $Rh(COD)(PPh_3)_2^+$ (Fig. 4) or $Rh(COD)(\mathbf{4})_2^+$ (Fig. 5) are similar, but the time scales are different. This is consistent with an interpretation that the ratios of rates, 1-hexene hydrogenation/1-hexene isomerization as well as 1-hexene hydrogenation/2-hexene hydrogenation, are similar for the two systems, but that the individual rates are faster for $Rh(COD)(\mathbf{4})_2^+$. The faster rates for the $Rh(COD)(\mathbf{4})_2^+$ catalyst are consistent with an interpretation that the aryldialkyl phosphine, **4**, is more basic and/or less sterically demanding of the rhodium coordination sphere than PPh_3. Similar observations were made by Schrock et al., for complexes containing PPh_3, PPh_2Me or $PPhMe_2$ [3].

A comparison of Fig. 5 and 6 illustrates significant differences in the relative

rates of hydrogenation as well as isomerization between the two isomeric catalyst systems involved. Relative to $Rh(COD)(\mathbf{4})_2^+$, the $Rh(COD)(\mathbf{3})_2^+$ system produces more isomerization and less hydrogenation. These differences may best be explained by the difference in steric requirements of the phosphine ligands **3** and **4** as discussed above. Differences in reactivity between $RhH_2(\mathbf{3})_2S_x^+$ and $RhH_2(\mathbf{4})_2S_x^+$ are not expected to be due to possible complexation of the olefin moiety of **3**, since attempts to prepare a chelated $Rh(COD)(7,8,9\eta^3\text{-}\mathbf{3})^+$ complex were unsuccessful. The less sterically demanding phosphine **3** allows for a greater probability of isomerization of 1-hexene to a more highly substituted olefin, due to lesser steric interactions between phosphine ligand and substrate in the transition state. Isomerization within the coordination sphere can occur at the expense of hydrogenation. The rate of disappearance of internal isomeric hexenes (after 1-hexene has been depleted) is much slower in the $RhH_2(\mathbf{3})_2S_x^+$ catalyzed reaction. This may be due to the ability of this complex to isomerize 2-hexenes to 3-hexenes in competition with hydrogenation of 2-hexenes to form n-hexane. The enhancement of the rate of 1-hexene hydrogenation catalyzed by rhodium complexes of **3** or **4** relative to PPh_3 parallels the enhancement of the rate of hydrogenation utilizing the aryldialkyl phosphine $PPhMe_2$ relative to PPh_3 [3].

In summary, we have shown that changes in inner coordination shell ligand orientations can be detected by variable temperature NMR by using rigid cyclic phosphine ligands which incorporate asymmetry about the Rh–P bond axis. By investigating two diastereomeric *meso* ligand forms we have been able to probe the influence of steric effects on ligand orientations and on 1-hexene hydrogenation/isomerization catalysis, while maintaining the same substituent groups on the P donor atom. Barriers to Rh–P bond rotations were found to vary with substituent orientation at the P donor atom. Differences in catalytic activity/selectivity as measured by 1-hexene hydrogenation and isomerization rates were found to parallel the influence of interligand steric effects on Rh–P bond rotation dynamics in these complexes.

Acknowledgements

Financial support from the North Carolina Biotechnology Center, the Office of Naval Research, and the University Research Council is gratefully acknowledged. This is a contribution from the North Carolina Biomolecular Engineering and Materials Application Center (NC-BEMAC) of which ALC is a member.

References

1 A.L. Crumbliss, R.J. Topping, J. Szewczyk, A.T. McPhail, and L.D. Quin, J. Chem. Soc., Dalton Trans., (1966) 1895.
2 R.S. Dickson, Homogeneous Catalysis with Compounds of Rhodium and Iridium, Reidel, Dordrecht, 1985.
3 R.R. Schrock and J.A. Osborn, J. Am. Chem. Soc., 98 (1976) 2134.
4 J.P. Collman, K.M. Kosydar, M. Bressnan, W. Lamanna, and T. Garrett, J. Am. Chem. Soc., 106 (1984) 2569.
5 D.R. Anton and R.H. Crabtree, Organometallics, 2 (1983) 855.
6 R. Cramer, J. Am. Chem. Soc., 89 (1967) 4621.
7 D. Bingham, D.E. Webster, and P.B. Wells, J. Chem. Soc., Dalton Trans., (1974) 1519.

8 J.L. Graff, R.D. Sanner, and M.S. Wrighton, Organometallics, 1 (1982) 837.
9 R.L. Pruett and J.A. Smith, J. Org. Chem., 34 (1969) 327.
10 M. Green, T.A. Kuc, and S.H. Taylor, J. Chem. Soc. A, (1971) 2334.
11 T.J. Katz, C.R. Nicholson, and C.A. Reilly, J. Am. Chem. Soc., 88 (1966) 3822.
12 M. Green, T.A. Kuc, and S.H. Taylor, J. Chem. Soc. A, (1971) 2234.
13 E.W. Turnblom, and T.J. Katz, J. Am. Chem. Soc., 95 (1973) 4292.
14 J.A. Berson, M.S. Poonian, and W.J. Libbey, J. Am. Chem. Soc., 91 (1969) 5567.
15 L.D. Quin and K.A. Mesch, J. Chem. Soc., Chem. Commun., (1980) 959.
16 L.D. Quin, K.C. Caster, J.C. Kisalus, and K.A. Mesch, J. Am. Chem. Soc., 106 (1984) 7021..
17 L.D. Quin, N.S. Rao, R.J. Topping, and A.T. McPhail, J. Am. Chem. Soc., 108 (1986) 4519.
18 H. Shanan-Atidi and K.H. Bar-Eli, J. Phys. Chem., 74 (1970) 961.
19 J.M. Brown, P.A. Chaloner, A.G. Kent, B.A. Marrer, P.N. Nicholson, D. Parker, and P.J. Sidebotton, J. Organomet. Chem., 216 (1981) 263.